



# NEAR Laser Rangefinder: A Tool for the Mapping and Topologic Study of Asteroid 433 Eros

Timothy D. Cole

In 1999, after a 3-year transit through space, the Near Earth Asteroid Rendezvous (NEAR) spacecraft will place a scientific payload consisting of five instruments into a low-altitude orbit ( $\approx 35$  km) about the asteroid 433 Eros for 1 year. One instrument, the NEAR Laser Rangefinder (NLR), will use infrared laser pulses to provide astrophysicists with precision altimetry data, measurements that were previously unavailable from asteroid observations. These data will accurately map Eros's topology, identify and characterize small-scale surface features, and precisely determine overall volume and mass once they are combined with navigation data. Objectives associated with the NLR science mission are presented along with performance specifications and instrument design details. The method by which NLR performance was analyzed is described, as are tests used to verify its performance and operability. During performance testing, an "end-to-end" test was conducted, where the integrated NLR instrument was operated in free space using a 216.4-m hallway. Test results fully verified all instrument interfaces and indicated that NLR performance parameters were well within all specifications. In addition, range noise and biases were repeatable to 1 count, which is the minimum level possible for a direct-detection rangefinder.

(Keywords: Acceptance testing, APD detector, Laser altimeter, Laser Rangefinder.)

## INTRODUCTION

On 17 February 1996, NASA's first Discovery mission began as the Delta II rocket rose from complex 17B carrying the Near Earth Asteroid Rendezvous (NEAR) spacecraft. The overall NEAR mission objective is to provide information about the origin and nature of near-Earth asteroids, whose characteristics are suspected to provide clues about the formation of the inner planets, including the Earth, and whose composition is reflective of material as it existed soon after the "big bang." Interest in asteroids has been further heightened by the realization of their potential

for terrestrial impacts; the Earth's geologic record contains evidence of many such events, including the cataclysmic collision that occurred some 65 million years ago.

Astrophysicists have derived their knowledge of asteroids from Earth-based observations, distant spacecraft flybys, and analyses of meteorites. From these data, a framework was developed to theoretically model asteroidal dynamics, structure, and thermal evolution. Indeed, sizes and shapes of asteroids contain important clues about their thermal, collisional, and

dynamic histories and their internal structures. The NEAR mission offers an opportunity to dramatically improve our understanding of asteroids by gathering data in close proximity to one. In addition to gathering data typical of previous observations, the NEAR mission will obtain asteroid data never possible before, data whose gathering requires close-range operation such as high-precision altimetry.

High-precision altimetry data will contribute significant insight to asteroid evolution by describing surface characteristics and global parameters such as volume and mass. The altimeter instrument, the NEAR Laser Ranging Finder (NLR), is designed to operate continuously throughout the 1-year orbit and to produce precision altimetry data over altitudes  $<327$  km from Eros's surface. This laser altimeter detects round-trip time, or time of flight (TOF), using a high-power pulsed laser with precise (2.08-ns resolution) timing measurements, which provides range resolution of  $\approx 32$  cm. With onboard calibration capability and from instrument-level tests prior to launch, the NLR range accuracy is also  $\approx 32$  cm.

The target asteroid is 433 Eros, one of the largest and most intensively studied near-Earth asteroids. Astrophysicists have estimated Eros to be 10–20 km in size, with a rotational period of roughly 5.27 h and an albedo of 0.15. Available Earth-based observations<sup>1</sup> indicate that Eros is a highly elliptical body measuring  $36 \times 15 \times 13$  km. These data, however, do not rule out the possibility that Eros may actually be a “rubble pile” consisting of two or more small, gravitationally bound bodies. Figure 1 illustrates the geometry involved for NEAR. The instruments continually observe Eros by attitude rotation. The rotation plane is constrained by the requirements to maintain solar arrays, which are mechanically fixed, facing toward the Sun and to keep the high-gain antenna within an acceptable angle of Earth's position.

The NLR design approach is described in this article. The approach used to analyze the operating performance of the altimeter is presented, and results from this analysis are summarized. To validate the NLR design and to ensure its successful operation subsequent to launch and exposure to deep space over a total period of 4 years, several instrument-level and integration tests were devised and performed. These included an operational test of the NLR to verify correct system operation “end-to-end” and to characterize instrument

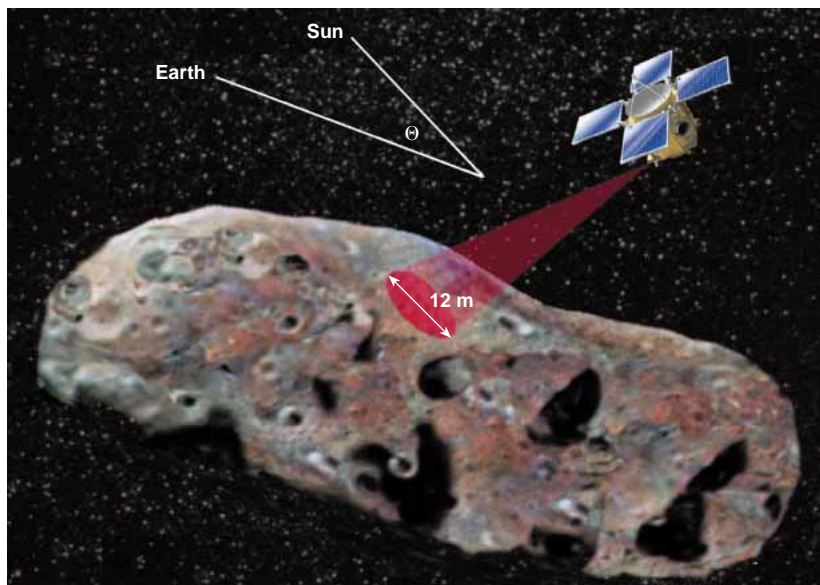


**Figure 1.** NEAR will place a spacecraft into orbit about the elliptical asteroid 433 Eros. The asteroid's dimensions have been estimated at  $36 \times 15 \times 13$  km. NEAR's optical instruments, including the laser radar, are continuously pointed toward the asteroid's surface. Critical angles must be preserved as the spacecraft orbits Eros and rotates to have the instruments face the asteroid's surface. These angles are governed by the requirement to maintain solar illumination of the power arrays and to remain connected with the Earth's communications network, the Deep Space Network.

bias and performance. End-to-end testing also provided information associated with operational peculiarities of the NLR and was vital to the check-out of the instrument's interface to the spacecraft.

## MISSION SPECIFICATIONS

The objective of the NEAR laser ranging investigation is to obtain accurate, high-resolution altimetry measurements that can be correlated with navigation and gravity data to provide quantitative insight into the internal structure, rotational dynamics, and evolution of Eros. According to Dr. Maria Zuber, the NLR science team leader, NEAR altimetry data and orbital tracking data will allow the volume and mass of Eros to be estimated to a precision of 0.01% and 0.0001%, respectively. Comparison between the NLR-derived data set and the predetermined gravity field (estimated from Eros's shape and spacecraft orbit perturbations) will permit correlation of surface topography to the local gravity field. Although the mean density measurement will be limited by the accuracy of our topographic field, resultant volume and mass values can be estimated with an accuracy significantly improved over that for any other asteroid previously observed.

Specifications for the NLR were derived from NLR mission requirements and spacecraft constraints. To provide the desired volume and mass measurement precision, single-shot altimetry resolution and accuracy relative to the asteroid center of mass must not exceed 6 m. For small-scale topology, altimetry sample density

(spacing between altimetry measurements on Eros's surface) must be almost contiguous along the direction of the subsatellite track on the asteroid. Over the range of spacecraft altitudes expected with a spacecraft velocity of 5 m/s relative to Eros, the sampling density will be more than adequate given the altimeter firing rate of 1 Hz and a laser transmitter divergence of  $235 \mu\text{rad}$ . Figure 2 illustrates the extreme expected orbit geometries and resulting sampling densities. In addition to the sampling density along the track, global parameter estimation requires that the cross-track resolution, that is, the spatial resolution perpendicular to the subsatellite tracks, must be  $\approx 500$  m. Cross-track resolution is governed by orbit-to-orbit separation and orbit (NLR) mission duration; therefore, it was not considered a direct requirement for the NLR instrument.

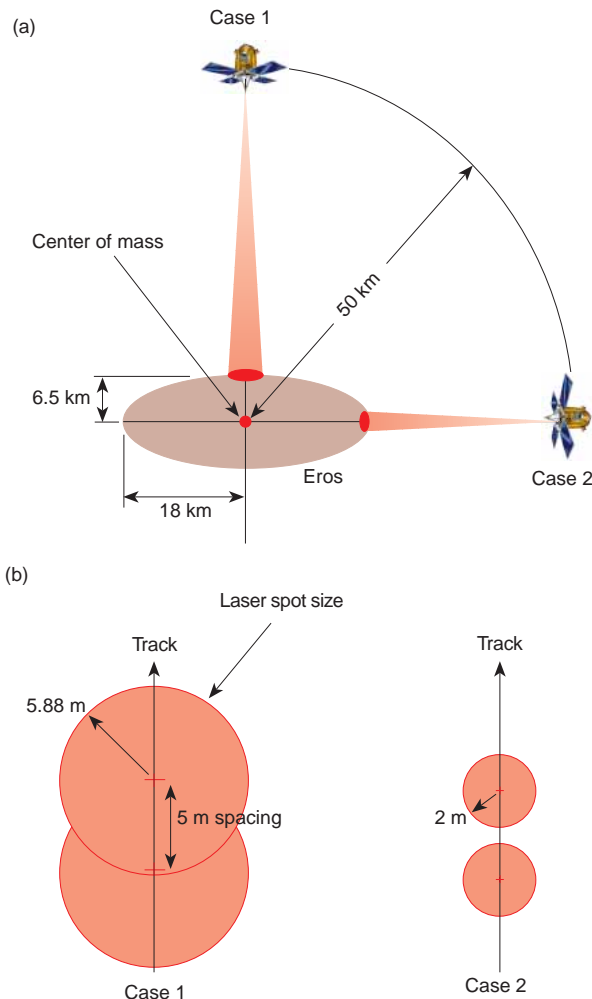


**Figure 2.** Mission geometry of the NEAR spacecraft during its encounter with the near-Earth asteroid 433 Eros. Two extreme orbital configurations are shown to demonstrate different perspectives. (a) The two extremes for the NEAR orbit geometry for the NLR. (b) The instrument's footprint and spacing dimensions. Case 1 shows the spacecraft orbit position relative to Eros's major axis, with significantly overlapped sampling. Case 2 shows ground track sampling, which is nearly contiguous.

All NLR measurements will be registered in an absolute center-of-mass reference frame, allowing precise registration with data from other NEAR sensors. Any offset between center of mass and center of figure for the asteroid will be determined by correlating gravity with topography data. The offset will reveal whether internal density differences are uniformly distributed and will help verify if Eros consists of two or more gravitationally bound bodies. Table 1 summarizes the requirements for the NLR based on NLR science objectives and on estimated characteristics associated with Eros.

## NLR SYSTEM DESIGN: A MODULAR APPROACH

To meet the accelerated schedule for the NEAR program, the NLR was developed as a modular system (Fig. 3). We selected a bistatic configuration, which permitted parallel development of the transmitter and receiver. The NLR instrument operates by transmitting laser pulses to the asteroid surface and measuring the TOF between outgoing light energy and optical energy backscatter from the asteroid surface toward the receiver. This direct-detection approach uses leading-edge detection based on Neyman-Pearson thresholding, thereby greatly simplifying wave form processing requirements. Not only are leading-edge altimeters relatively simple to implement, but the approach reduces range scintillation generated when the extent of the target range exceeds the transmitted pulse width, a condition that could be encountered when mapping irregular surfaces of an asteroid.

### Basic Subsystems and Operation

The NLR required 19 months to develop, from start of design through completion of flight qualification. The transmitter and receiver units were developed and tested separately; subsystems were tested prior to integration using National Institute of Standards and Technology (NIST)-traceable equipment. Although schedule constraints precluded fabrication of brass-board models, breadboard and engineering models were produced and used extensively to debug design and packaging issues.

A block diagram of the NLR instrument (Fig. 4) shows its five subsystems: the laser transmitter subassembly with a fiber-optic delay assembly (FODA) and laser power supply (LPS); the optical receiver; the analog electronics with a detector, processor boards, and a medium-voltage power supply (MVPS); the digital processing unit (DPU); and the low-voltage power supply (LVPS). Red lines in Fig. 4 indicate the optical paths for laser signals; red words indicate the primary signals for the electronics. The optical receiver, analog electronics, LVPS, MVPS, and DPU are collectively

Table 1. Specifications for the NLR instrument, determined through direct measurement or inferred from related measurements.

Parameter	Specification	Measurement <sup>a</sup> / Estimate <sup>b</sup>
Max. range (altitude)	50 km	>100 km <sup>b</sup>
Albedo (reflectivity)	0.10–0.22	0.15 <sup>b</sup>
Range accuracy	≤6m	<6 m <sup>b</sup>
Range resolution	≤6m	31.22 cm <sup>a</sup>
Instrument weight (max.)	5 kg	4.9 kg <sup>a</sup>
Instrument power (avg.)	<22 W	15.1 W <sup>a</sup>
Sample (grid) spacing	Contiguous	Contiguous (overlapped) <sup>a</sup>
Data rates	<10 to <56 bps	Variable; 6.4–51 bps <sup>a</sup>
Operational period	1 year (continuous)	N/A <sup>c</sup>
Lifetime	4 years	N/A <sup>c</sup>

<sup>a</sup>Actual measurements; <sup>b</sup>estimates using indirect measures; <sup>c</sup>not applicable.

referred to as the NLR receiver. The receiver was designed, fabricated, and tested at APL. The transmitter was obtained through subcontract from McDonnell

Douglas Aerospace Corp. The transmitter, once completed and qualified by McDonnell Douglas Aerospace Corp., was delivered to APL for final integration and acceptance testing at the instrument level. The integrated NLR instrument was subsequently tested and subsequently flight qualified at both instrument and spacecraft levels.

NLR operation is described by Fig. 4. The measurement sequence begins with a “Fire” command issued by the DPU at a selected pulse repetition frequency. This command enables the transmitter, which fires a 15-ns optical pulse toward the asteroid and simultaneously directs a portion of this pulse into the FODA for calibration

TOF purposes. A photodiode at the transmitter output detects the laser pulse and sends an electronic START signal command to both of the receiver

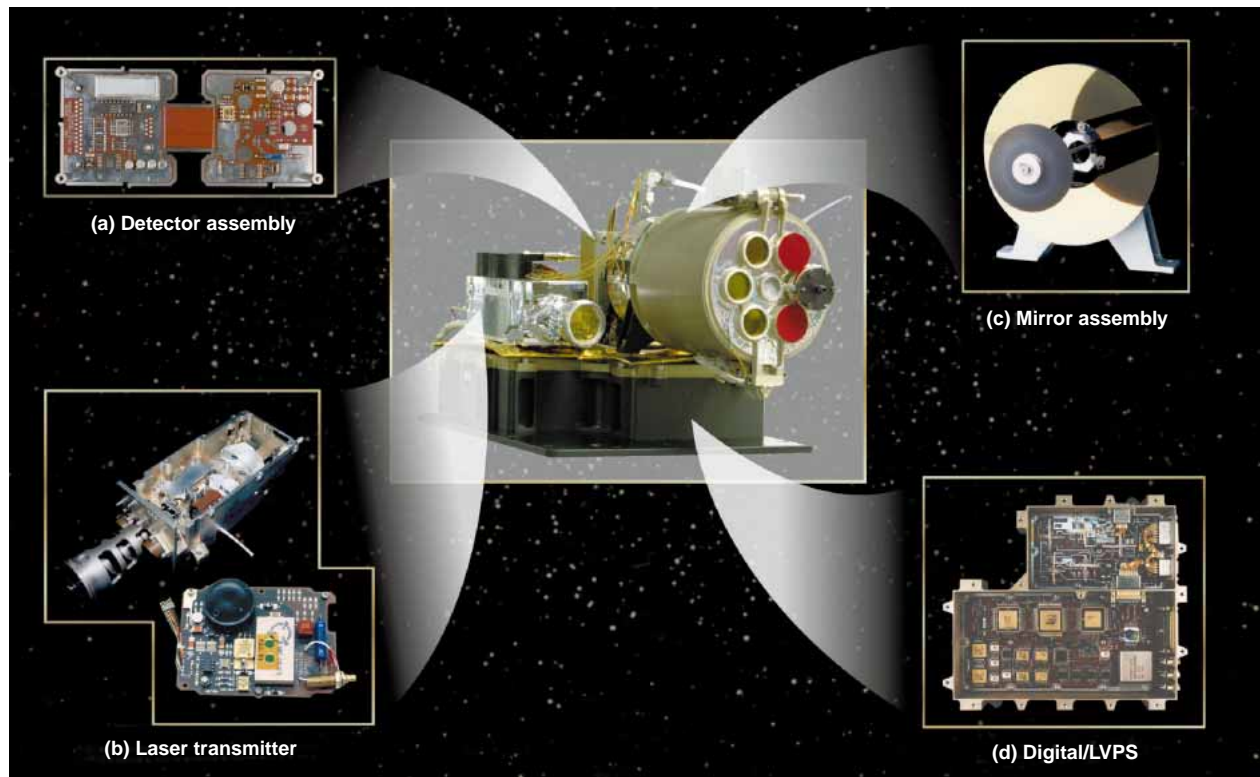


**Figure 3.** The integrated NLR instrument showing key subsystems. (a) The detector assembly uses an enhanced avalanche photodiode hybrid mounted at the receiver focal plane (the detector is on the opposite side as shown). (b) The laser resonator and associated laser power supply are based on previous designs. (c) Receiver optics (mirror assembly) consist of an all-reflective, lightweight Dall–Kirkham telescope made of aluminum (athermal design). (d) Receiver electronics are shown mounted in the NLR chassis; both the digital processing unit and the low-voltage power supply (LVPS) are shown. The calibration unit, a 109.5-m length of spooled optical fiber, is shown on top of the transmitter in the center photograph (black cylinder). Not shown is the avalanche photodiode power supply (+550 V DC) and the laser power supply; both were remotely located to minimize interference with the sensitive receiver electronics.

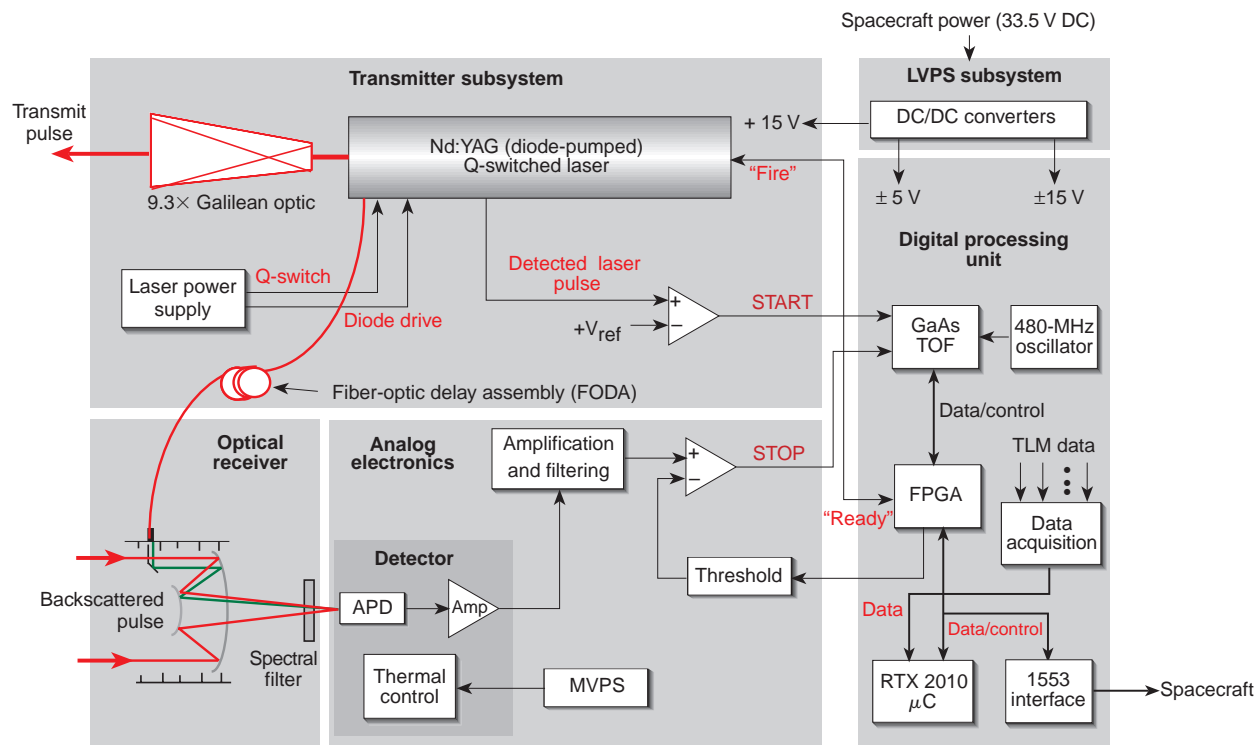


**Figure 4.** The five subsystems of the NLR instrument consist of the transmitter subsystem, the low-voltage power supply (LVPS), the optical receiver, the analog electronics, and the digital processing unit. Gray areas indicate these subsystems. Red lines indicate optical signals (laser light). Thresholding is used both to start the time-of-flight (TOF) counters (START) and to stop the same counters (STOP). APD = avalanche photodiode;  $\mu\text{C}$  = microcontroller; FPGA = field-programmable gate array; MVPS = medium-voltage power supply; TLM = telemetry data.

gallium arsenide (GaAs) TOF counters (range and calibration).

As a result, during operation, the NLR receiver should see two optical pulses per transmitted pulse. The first, arriving 558 ns after the laser fires, is a calibration pulse routed through the fixed delay provided by the FODA. Detection of this pulse by the receiver halts the calibration TOF counter. The second return is the optical backscatter from the asteroid, which halts the range counter. To minimize noise, received optical signals are compared with a threshold level set either by ground command or through an auto-acquisition (calibration) sequence. After both TOF counters are stopped, the DPU reads the counter values and formats their contents (and other data) into NLR science data packets for transmission over the 1553 bus, as requested by the spacecraft data collection process. Consequently, what is measured is elapsed time between the START indication from the laser and the arrival of STOP signals as produced within the receiver. Terms used in Fig. 4 are defined and described in subsequent sections. The figure also illustrates the electrical interface between the spacecraft and the instrument. (Heater control and receiver door release circuits are not shown.)

## NLR Transmitter

The laser resonator assembly (LRA) is a solid-state laser based on a proven polarization-coupled U-cavity design<sup>2</sup> (Fig. 5). The gain medium is a Cr:Nd:YAG zigzag slab, side-pumped at 809 nm using a 20-element gallium arsenide (GaAs) diode array (having thermal sensitivity of  $\Delta\lambda/\Delta T = 1 \text{ nm}/4^\circ\text{C}$ ) with a peak power of 620 W in a pulse width of 200  $\mu\text{s}$ . The opposite side of the slab is coupled to a heat sink for thermal control. An antireflection coating applied to the long dimension of the slab improves pump-power coupling efficiency, and a high reflectance coating on the heat-sink side reflects pump energy back into the slab. This zigzag pumping yields a uniform distribution of optical energy throughout the gain medium, increasing absorption path length and conversion efficiency.

An antireflection coating at both slab end faces reduces optical losses for rotated polarization states. A quarter-wave plate placed after the slab end face maintains polarization. The gain medium is located in a cross-porro cavity to provide boresight stability; a Risley wedge in each porro prism assembly permits cavity alignment during assembly. An internal aperture reduces higher-order modes, and a 9.3x Galilean telescope acts as an external beam expander to reduce

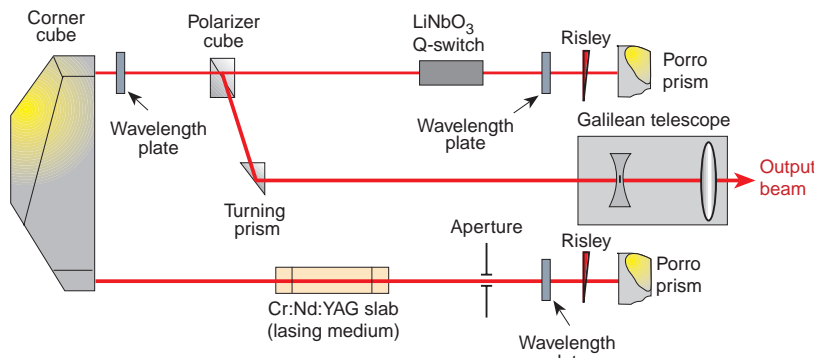


**Figure 5.** NLR laser resonator cavity configuration is a polarization-coupled U-shaped cavity design.<sup>2</sup> The Cr:Nd:YAG zigzag slab is side-pumped by a diode laser array to optimize conversion efficiency.

angular divergence. (Output beam divergence was specified as  $\leq 300 \mu\text{rad}$ ; our final divergence, in vacuum, is  $235 \mu\text{rad}$ .)

The laser operates at  $1.064 \mu\text{m}$  and is Q-switched for pulsed-mode operation using a lithium niobate ( $\text{LiNbO}_3$ ) Pockels cell. A half-wave plate provides polarization compensation. Placement of the Q-switch in the output segment of the beam path minimizes the potential for optical damage to the crystal by locating it within the low circulating power portion of the resonator. Because  $\text{LiNbO}_3$  is pyroelectric, thermal gradients must be controlled during operation in vacuum environments. For this reason, the NLR has redundant operational and survival heater circuits to reduce thermal variations to  $-2$  to  $+4^\circ\text{C}$  of the thermal set point.

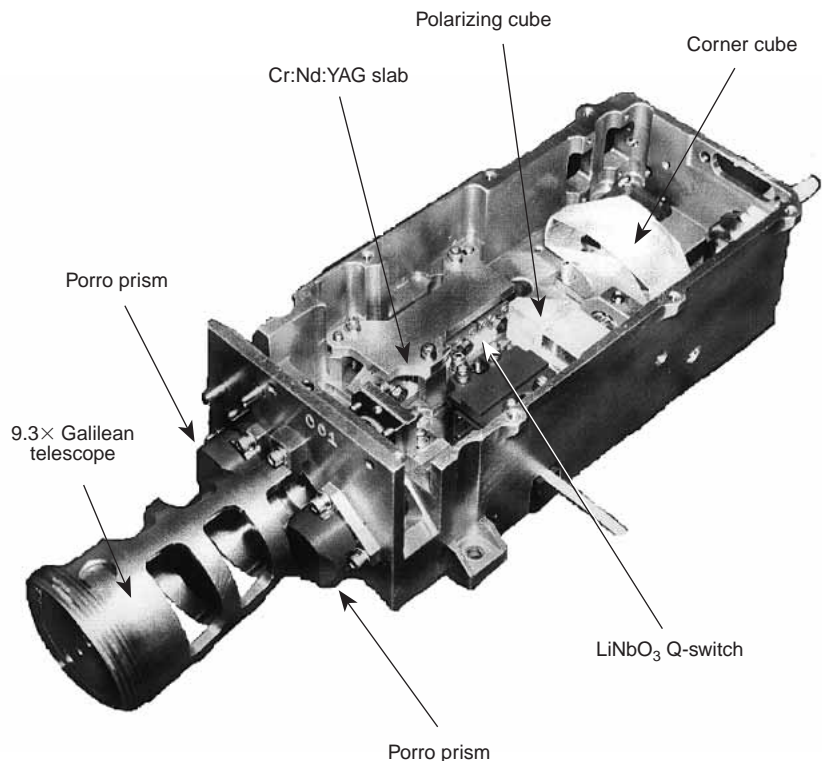
To provide thermal isolation, the LRA is mounted to the NLR housing using Vespel shoulder washers. Figure 6 is a photograph of the actual LRA assembly depicting the laser and associated resonator optics. Note the lightweight  $9.3\times$  output optic. Mechanical interface for the LRA uses a three-point kinematic mounting configuration.

Table 2 presents specifications for the NLR. Also presented are measurements (and estimates) for each of these values. The laser transmitter was extensively characterized as part of the NLR instrument test sequence. The system reliably produced  $15\text{-ns}$  ( $\pm 0.82 \text{ ns}$ ) optical pulses each having  $15.3 \text{ mJ}$  ( $\pm 2 \text{ mJ}$ ) energy. This optical pulse was coupled to the FODA and was measured at the LRA output coupler as  $7.2 \text{ pJ}$ . (All

power measurements used NIST-traceable power meters accurate to  $\pm 5\%$ ). Prelaunch NLR testing demonstrated that the NLR passed all specifications.

The output beam was characterized using a fast (picosecond response) detector to detail the longitudinal mode structure (Fig. 7). Characterization of the near field included measurement of beam diameter (defined where amplitude decreases to  $1/e^2$  of maximum), modal structure, and energy distribution. Far-field testing consisted of beam divergence,

jitter, and wander. Divergence significantly affects the science data through surface sampling size. This parameter was measured in both air (ambient, at  $135 \mu\text{rad}$ ) and vacuum ( $235 \mu\text{rad}$ ) (Fig. 8). Gaussian correlation coefficients along both the  $x$  and  $y$  axes were  $0.91$ ; therefore, performance was better than the specified  $0.90$ . The difference in divergence is related to output telescope alignment with and without atmosphere. Although the index of refraction changes by only 3 parts in 10,000,<sup>3</sup> it was enough in a high-power



**Figure 6.** The LRA optical component configuration. Note the lightweight structure, made of aluminum, used to mount the elements for the Galilean beam expander. One side uses metallic Mylar for electromagnetic compatibility/electromagnetic interference purposes (bottom of unit). Mechanical mounting is 3-point kinematic.

Table 2. NLR design parameters.

Parameter	Specification	Measurement <sup>a</sup> / Estimate <sup>b</sup>
Transmitter pulse energy	>5 mJ @ 1.064 $\mu\text{m}$	15.6 mJ <sup>a</sup>
Transmitter energy jitter	<10%	<1% <sup>a</sup>
Transmitted pulsewidth, $t_{\text{pw}}$	10 ns < $t_{\text{pw}}$ < 20 ns	15 ns <sup>a</sup>
Transmitted pulsewidth jitter	<2 ns	0.82 ns <sup>a</sup>
Transmitter wavelength broadening	$\pm 3$ nm	$\pm 1$ nm <sup>a</sup>
PRF rates	1/8, 1 (nominal), 2, 8 Hz	1/8, 1, 2, 8 Hz <sup>a</sup>
Range gate (resolution)	N/A <sup>c</sup>	0.00–42.63 $\mu\text{s}$ (41.67 ns) <sup>a</sup>
T-0 event mask (resolution)	N/A <sup>c</sup>	0.00–511.50 $\mu\text{s}$ (500 ns) <sup>a</sup>
TEM00 mode (% Gaussian)	>90%	91% <sup>a</sup>
Divergence ( $1/e^2$ )	<300 $\mu\text{rad}$	235 $\mu\text{rad}$ <sup>a</sup>
Beam waist (near-field)	N/A <sup>c</sup>	22.93 $\pm$ 0.12 mm <sup>a</sup>
Beam centroid jitter (shot-to-shot)	<50 $\mu\text{rad}$	16.31 $\pm$ 24.39 $\mu\text{rad}$ <sup>a</sup>
Beam centroid wander	<300 $\mu\text{rad}$	4.81 $\pm$ 31.25 $\mu\text{rad}$ <sup>a</sup>
Calibration power jitter	$\pm 5\%$	<5% <sup>a</sup>
Calibration timing jitter	<1 m	<31.22 cm <sup>a</sup>
Thermal control	$\pm 2^\circ\text{C}$	$\pm 2^\circ\text{C}$ <sup>a</sup>
Shots (lifetime)	>31.5 $\times 10^6$	>1 $\times 10^9$ (TBD)
Effective aperture, $f/\#$	N/A <sup>c</sup>	7.62 cm, $f/3.4$ <sup>a</sup>
Spectral receiver bandwidth	<10 nm	7 nm <sup>a</sup>
Temporal receiver bandwidth	$\leq 100$ MHz	30 MHz <sup>a</sup>
APD dark voltage	$\leq 195$ $\mu\text{Vrms}$ (24 MHz bandwidth)	150 $\mu\text{Vrms}$ (24 MHz bandwidth) <sup>a</sup>
APD responsivity	$\geq 770$ kV/W	775 kV/W <sup>a</sup>
Optical receiver FOV	>900 $\mu\text{rad}$	2.9 $\mu\text{rad}$ <sup>b</sup>
Threshold levels	N/A <sup>c</sup>	8 ( $2^n \times 16$ mV, $n = 0$ to 7) <sup>a</sup>
Data rates	51 bps, 6.4 bps	Variable, including 51 and 6.4 bps <sup>a</sup>
TX-to-RX alignment shift	<1100 $\mu\text{rad}$ (700 $\mu\text{m}$ effective diameter APD)	345.0 $\mu\text{rad}$ <sup>a</sup> (pre- to post-values vibration test)

Note: APD = avalanche photodiode; FOV = field of view; PRF = pulse repetition frequency; TBD = to be determined; T-0 = laser firing time; TEM00 = transverse electromagnetic wave fundamental mode.

<sup>a</sup>Actual measurements; <sup>b</sup>estimates using indirect measures; <sup>c</sup>not applicable.

optic using air-gap spacing to make a measurable difference in the wavefront shaping.

The LPS provides the control logic and power necessary to enable and fire the LRA. The LPS also provides the 190- $\mu\text{s}$  pump current (45 A) to the diode array. A hybrid component develops the +2800 V necessary to operate the Q-switch. Upon receiving a “Fire” command from the DPU, the LPS uses a signal from the NLR logic within the DPU to begin charging the storage capacitors that produce the diode drive current. To reduce noise coupling to the receiver during expected arrival of laser backscatter, the switching DC/DC converter within the LPS is disabled for the maximum ranging distance (327 km). Subsequent to maximum TOF, the LPS is enabled to prepare for the next pulse.

## NLR Receiver

The NLR receiver design uses a lightweight Cassegrain telescope, a spectral filter (centered at the laser wavelength), a single-element avalanche photodiode (APD) hybrid detector, amplification filtering, voltage biasing and thresholding circuitry, and appropriate power supplies (+550 V DC for the APD from the MVPS, and  $\pm 15$  V DC and  $\pm 5$  V DC from the LVPS). The receiver design was based on previous APL APD-based detection circuit designs and on APL developments in TOF systems using high-speed (2 GHz) GaAs applications-specific integrated circuitry (ASIC).

A significant aspect of our configuration is that the NLR receiver optics act as a direct-detection “photon bucket.” This approach drastically simplified the design and development of the optical receiver because

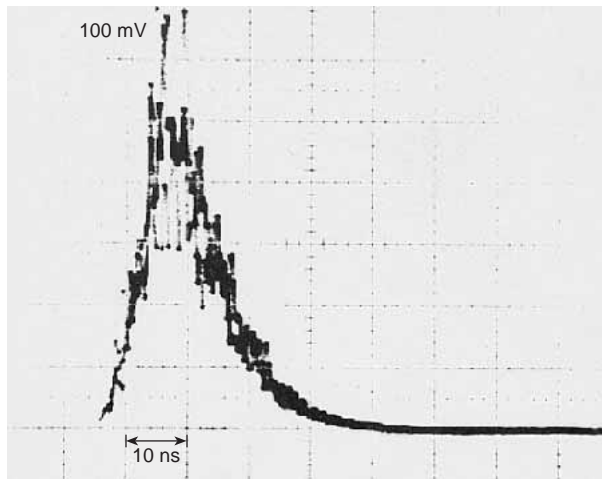


**Figure 7.** Temporal response of an LRA optical pulse. Each temporal unit represents 10 ns; full-width half maximum measures  $15 \pm 2$  ns. Longitudinal modes are present because the cavity is single mode only through aperturing.

the system is not required to produce an image. Consequently, the optics could tolerate high levels of aberrations as long as the resultant spot size remained within the physical and alignment bounds of the APD detector. This gave us the freedom to select the receiver optical design best suited for low weight and manufacturing ease, specifically, an  $f/3.4$  Dall-Kirkham design (Fig. 9).

Our telescope is a two-mirror aluminum Dall-Kirkham arrangement using an athermal design. The primary mirror is 3.5 in. (8.89 cm) (see Fig. 9) with an overall field of view of 3 mrad. The Dall-Kirkham layout is simple to manufacture but suffers primarily from coma arising from off-axis light. However, since the NLR operates with paraxial light, comatic aberration is minimal and does not influence the performance of the receiver.

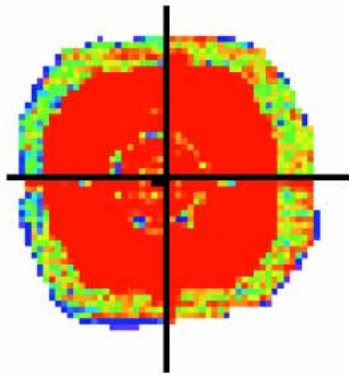


**Figure 8.** Ambient far-field pattern of a typical NLR pulse ( $135 \pm 2 \mu\text{rad}$  at  $1/e^2$  points). The beam pattern, which approaches a Gaussian intensity distribution, was acquired during ambient testing at the nominal pulse repetition frequency (1 Hz) and spacecraft voltage (33.5 V). Vacuum divergence measured  $235 \pm 2 \mu\text{rad}$ .

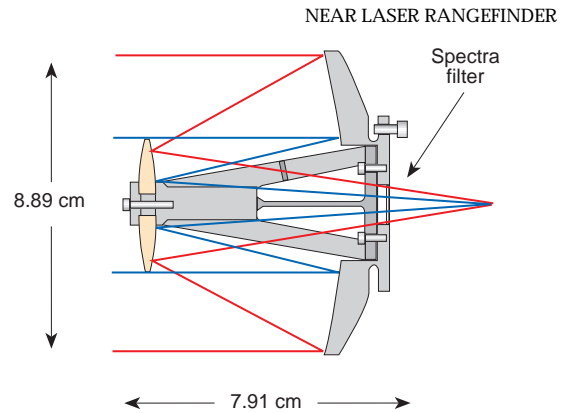


**Figure 9.** Dall-Kirkham, athermal (aluminum) design for the NLR  $f/3.4$  receiver telescope. All optical surfaces were diamond-turned for NLR use. Overall weight of this telescope was 167.4 g.

Since there are no bright sources near the NLR line of sight when viewing Eros, specifications of surface roughness for the aluminum mirrors were relaxed; we used diamond-turned surfaces, which are relatively inexpensive for the mechanical and optical quality provided. No superpolishing was required; only an antioxidant layer was deposited onto the surfaces to maintain reflectivity. Stray light contamination was controlled by a system of baffles in the receiver support structure to prevent off-axis light from reaching the primary mirror in less than two reflections. The two-reflection tolerance reduced the number of baffles, and hence, the weight of the receiver housing. Baffles, made of lightweight magnesium, were also knife-edged to minimize direct reflections into the receiver telescope.

The final mass of the telescope assembly (Fig. 9) was 167.4 g. Acceptance testing indicated that 98% of the focused energy was located within a  $100\text{-}\mu\text{m}$  central (Airy) disk, easily accommodated by the  $700\text{-}\mu\text{m}$  active diameter of the APD detector.

To further reduce optical background noise, we placed a narrowband (7 nm) spectral filter in the convergence cone of the telescope, a location selected to reduce weight and cost. Spectral filter passbands are strongly dependent on temperature and angle of incidence. To minimize thermally induced performance variation, the filter was fabricated using a proprietary deposition process<sup>4</sup> that reduces passband shift by a factor of 10. We reduced angular sensitivity by selecting a wide enough passband to allow light from all angles of the telescope, where the converging cone of light at the detector extends from  $4$  to  $9^\circ$ , to pass with minimal attenuation. The relatively low orbital velocity of the spacecraft (5 m/s) imposed negligible Doppler requirement on filter bandpass performance.

A windowed door over the entrance aperture of the NLR receiver protects the optics from contamination. Our primary concern was contamination from byproducts arising from propellant burns during the transit

phase, but the door also provided mechanical and contamination protection during prelaunch activities. The door is a deployable element meant to be opened once, which was successfully accomplished on September 24, 1997. Both transmitter and receiver optical sections were kept under a positive purge using research-grade nitrogen prior to launch with a purge valve in the receiver door for pressure relief. (The transmitter did not require a door; however, the transmitter was nevertheless kept under purge until final pressure equalization was reached subsequent to launch.) The door-release mechanism uses redundant pyrotechnic wire cutters with a tempered beryllium oxide wire. Six silica-coated windows are located on the receiver door to provide approximately 50% of the total collecting area in the event of a door-release failure at Eros. This 50% collection area will permit the NLR to operate at the planned orbital altitude (50 km).

### Analog Electronics

The purpose of the analog electronics is to convert backscattered optical energy from the asteroid surface into a digital STOP signal, permitting round-trip TOF measurements to be computed. Four fundamental stages compose the analog electronics (Fig. 10): the APD hybrid detector, a video amplifier, an integrator stage (Bessel-type lowpass filter), and a programmable comparator. The detector and amplifier are installed on a rigid-flex detector board where the detector electronics use 50- $\Omega$  matched lines; the integrator and comparator are installed on a separate, analog signal processing board.

The APD is a hybrid device combining an enhanced silicon APD with temperature compensation and transimpedance amplification. The enhancement process pushes maximum response of the APD detector slightly beyond 1  $\mu\text{m}$ . The particular APD used for the NLR is a wide field-of-view (FOV) detector with a measured bandwidth response of 37 MHz and responsivity of 770 kV/W. (For coherent laser radars, electronic bandwidth of the baseband signal relates to the FOV used in observing the returned signal.) Assuming 15-ns pulses at 1.064  $\mu\text{m}$ , our detector circuit operates with a minimum detectable power of 9 nW and maximum input power of 0.5 W. Gain variation is less than 5% over the temperature range from  $-8$  to  $+40^\circ\text{C}$  due to compensation; however, our analog electronics housing is thermally controlled to  $20 \pm 10^\circ\text{C}$ .

The video amplifier stage consists of a wideband amplifier used to provide a gain of +50 over a 75-MHz bandwidth. The filtering, or integrator, stage is a seven-pole lowpass Bessel filter with 3-dB cutoff at

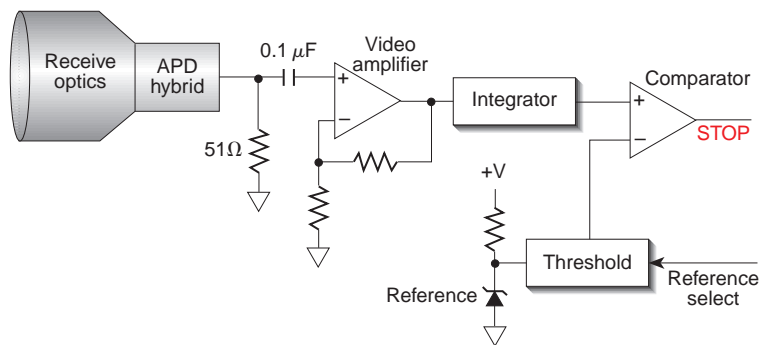


**Figure 10.** Analog processing block diagram. The analog signal was generated by a hybrid avalanche photodiode detector (APD) that included a transimpedance amplifier and thermal compensation. Filtering (integrator) was used to counteract pulse dilation effects. The filter used was a 7-pole low-pass Bessel filter (integrator). The threshold circuit (comparator) operated at one of eight levels, which are binary multiples of 16 mV.

30 MHz. The lowpass filter is used to integrate return pulses that may be spatially diluted by interaction of the transmitted laser pulse with the asteroid's topology. The use of this filter optimizes the probability of detection of anticipated surface slopes while it limits high-frequency noise response of the analog electronics.<sup>5</sup>

A comparator stage determines whether an input signal has sufficient energy to generate a STOP signal. The comparator operates using one of eight preset threshold levels, which are set by ground command or auto-thresholding. These threshold levels vary from 16 to 2048 mV; the lowest threshold is below the receiver noise floor, and the highest setting is just above the signal strength associated with the calibration input. Therefore, threshold levels increase as  $2^n V_{\text{th}}$ , where  $n = 0, \dots, 7$  and  $V_{\text{th}}$  is the threshold voltage (16 mV). Thresholding permits an input dynamic range of 24 dB to compensate for instrument noise sensitivity and variations of return signal strength. The comparator exhibits very low propagation delay ( $<2$  ns) and very little overdrive dispersion, making it ideal for precise timing applications such as leading-edge detection.<sup>6</sup>

### Digital Processing Unit

To save weight and to minimize high-speed lines to the TOF chip, the DPU uses a single rigid-flex multi-layered board (see Fig. 11). The board contains a GaAs TOF chip, a radiation-hardened RTX-2010 FORTH-language microcontroller, a dual-frequency stable oscillator, a field-programmable gate array (FPGA) chip, a redundant-channel 1553 chip set and attendant transformers, digital memory, an analog-to-digital (A/D) converter and sampler, and control logic.<sup>7</sup> The dual-frequency oscillator produces two output frequencies: 480 MHz  $\pm 0.01\%$  and 48 MHz  $\pm 0.01\%$ , with short-term (100  $\mu\text{s}$ ) frequency stability of 1:10<sup>8</sup>, but only the 480-MHz frequency is used. The required 48-MHz clock is generated using the 480-MHz

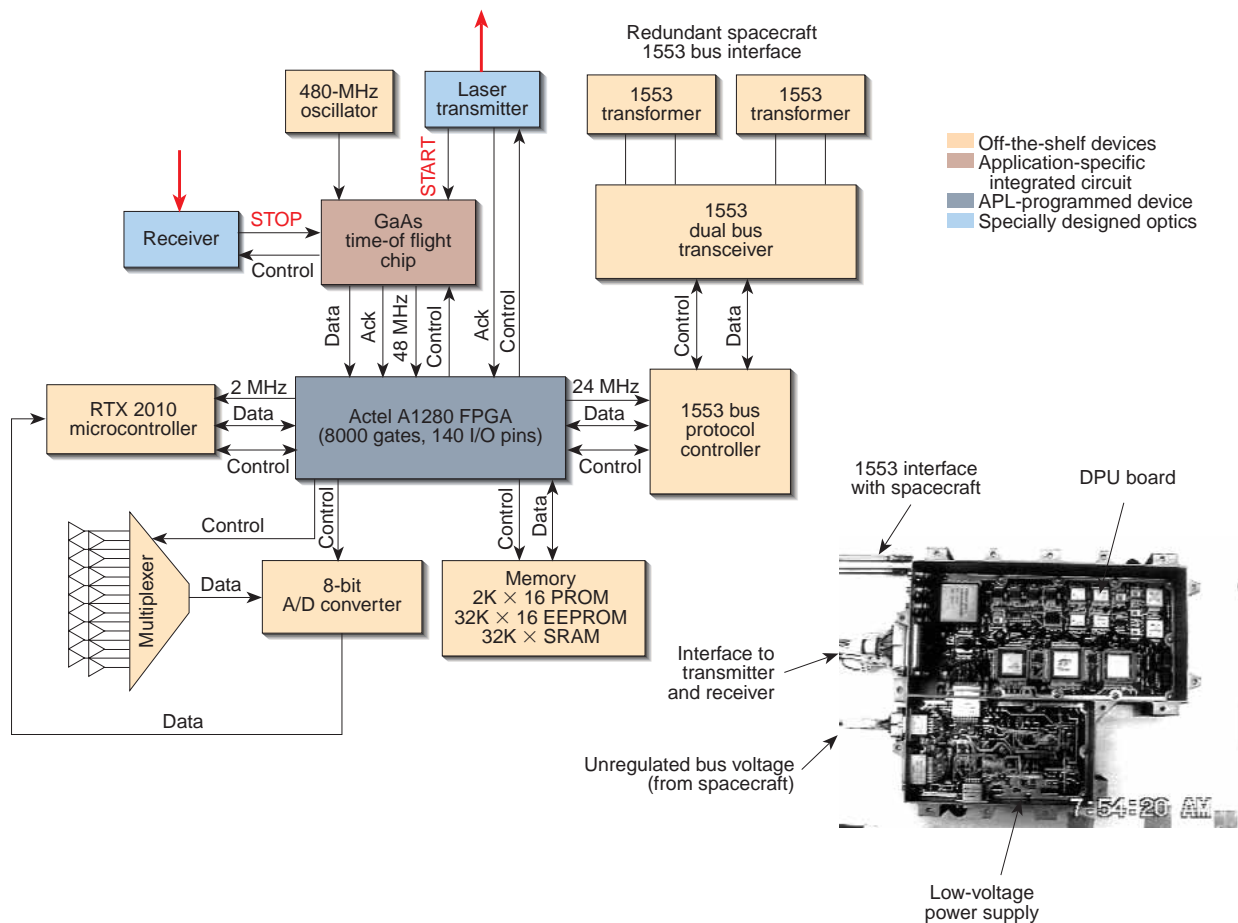


**Figure 11.** Digital processing unit (DPU) single-board implementation contains a GaAs time-of-flight chip, a radiation-hardened FORTH-language microcontroller, memory, an analog-to-digital (A/D) converter and sampler, redundant, redundant-channel 1553 chip set and attendant transformers, a dual-frequency stable oscillator, a field-programmable gate array (FPGA) chip, and control logic. The photograph shows DPU and low-voltage power supply boards as they appeared in the NLR chassis. An optical bench was mounted to this chassis, and the receiver and laser transmitter were aligned and mounted to this bench. Various in/out (I/O) ports are identified.

frequency within the TOF ASIC. The FPGA uses this 48-MHz clock and produces 24-MHz, 2-MHz, and 500-kHz output clocks for the 1553-bus controller, RTX microcontroller, and FPGA internal range-gating counters, respectively.

The GaAs TOF chip is an APL-designed ASIC with one 11-bit counter (used for calibration) and one 21-bit counter (used for range measurement with 1-bit overflow). Both counters operate at 480 MHz. The TOF counters are enabled with a “start” pulse from the transmitter (START) and are stopped when a detected return pulse arrives from the receiver comparator (STOP). The RTX-2010 is a parallel 16-bit microcontroller that operates at 2 MHz to conserve power. The microprocessor chip contains three on-chip timers, a dual-stack architecture, and an interrupt controller with the ability to handle five external interrupts.

The 1553-bus interface to the DPU consists of two 1553 bus transformers (channels A and B), a 1553 dual bus transceiver, and a bus protocol controller. The controller responds to bus commands sent by the

spacecraft command telemetry processor (CTP). The bus controller handles data transfers, commands, and telemetry that transfer between the NLR and the CTP. Data bus arbitration is handled by our FPGA, which simplified digital hardware design and fabrication by incorporating several functions such as address decoding, memory arbitration, clock generation, receiver range gating, receiver enable (denoted T-0 masking), and transmitter and receiver configuration control.

T-0 masking is necessary to eliminate spurious noise that is produced with the formation of the laser optical pulse. T-0 masking is a disabling of the range counters (both calibration and return signal counters) for a few cycles of the natural response of the receiver circuit at the time the optical pulse is formed within the laser transmitter. Without such masking, opportunities for false STOP signals are possible, and actual range measurements would not be possible. A second range-gating function is implemented to gate the return signal to improve the sensitivity of the NLR receiver.

The sought-after signal is the STOP indication, which is used to indicate a detected optical pulse above the set threshold. STOP terminates either the calibration or range TOF counter, depending on system configuration, and the corresponding range is read out.

## Software

The NLR software was programmed using the FORTH programming language for the RTX-2010 microcontroller. The software interfaces with the spacecraft CTP via the 1553 bus, executes commands from the ground control, formats science telemetry and instrument housekeeping commands, and controls instrument operation. The software was implemented in a multitasking environment running four different NLR programs<sup>8</sup>: (1) "NLR\_PROCESS" handles transmitter/receiver control and data formatting; (2) "TELEMETRY\_PROCESS" implements necessary 1553 protocol for data transfer; (3) "COMMAND\_PROCESS" handles incoming instrument commands; and (4) "DUMP\_PROCESS" transfers blocks of NLR memory to the telemetry stream for transmission to the ground.

"NLR\_PROCESS" is the main controlling program for the instrument. This task has the highest priority and requires 5 ms to execute. On the basis of a minor frame interrupt (every 125 ms) arriving by the 1553 bus, this program determines when to fire the transmitter, initialize receiver parameters (i.e., T-0 mask, threshold level, and receiver range-gate), and read and format calibration and range counter values (i.e., the altimetry measurements). Measurement data, spacecraft time, and NLR configuration parameters are formatted into a science packet for each transmitter shot, with 56 shots (112 for a pulse rate of 2 Hz) accumulated into each of these packets for transmission to ground via the downlink.

"NLR\_PROCESS" is programmed with several calibration algorithms. Operating during a contingency, or "fail-safe," mode, the TOF counter is started by a delayed transmitter fire command as opposed to an electronic trigger from the transmitter photodiode. This fire command is purposely delayed due to an inherently variable delay in the transmitter optical output, nominally 192  $\mu$ s. We can determine this delay by initiating a calibration mode that varies the T-0 mask through a 10-bit programmable counter until a reasonable calibration range is detected. Since the counter has a 500-ns resolution, the maximum range error due to a failed START would be 74.9 m.

The calibration algorithm configures the NLR to step through each threshold level and collect 16 samples of range and calibration data at a rate of 8 Hz. Collecting range data at 8 Hz minimizes the influence of relative movement between the NLR and asteroid terrain, permitting high correlation between data

points. This is important as range rate is calculated for each new sample at each threshold and is compared to a predetermined difference (sent as a command argument) to determine the system noise floor and, hence, the operating threshold for reliable range returns. The 8-Hz mode occurs for a 2-s burst followed by a 14-s quiescent period to reduce thermal stresses within the transmitter. Following the 14-s pause, the NLR automatically reconfigures to the nominal 1-Hz rate.

## In-line Optical Calibration

The NLR is the first laser altimeter to feature in-line calibration, which was implemented using a 109.5-m single-mode fused silica optical fiber. This fiber optic delay assembly (FODA) is optically connected between the transmitter and receiver using small turning mirrors and graded-index lens assemblies. A minute portion of each transmitted pulse is injected (using internal transmitter scattering at the corner cube, see Fig. 5) into the FODA, producing a constant optical delay of 529.20 ns between transmitted pulse and reception of that pulse by the receiver optics; the measured delay after integration into the system was 558.33 ns, indicating an additional system bias of 29.13 ns. By directing each transmitted optical pulse directly to the receiver optics, "true" end-to-end calibration is possible, which allows detection of range-walk, an error caused by threshold-level changes or oscillator drift. This self-calibration feature, therefore, ensures high quality of the NLR data and permits evaluation of the NLR instrument functionality throughout the mission. With the existence of the FODA, we essentially provide the NLR with a virtual fly-along laser radar target. This allows us to operate the NLR and obtain calibration measurements based on actual TOF readings using laser output power until our arrival at Eros.

In addition to instrument operation, the FODA proved invaluable for performance evaluation and debugging during prelaunch integration and test phases. Using the calibration range counter during testing allowed us to determine the quality of the instrument measurements based on threshold level selected, power levels used, operational mode selected, and various environmental conditions.

## NLR PERFORMANCE ANALYSIS

Performance was estimated using several approaches, including the basic radiometric modeling (Neyman-Pearson detection) and Webb's<sup>9</sup> photoelectron output approximation. Determination of the adequacy of the NLR design requires evaluation of performance given parameter values describing Eros, NLR mission parameters (e.g., orbit altitude), and the NLR design implementation. (Table 1 summarizes these parameters

describing the NLR design.) Analytical evaluations used these values to examine expected NLR performance through link margin calculations.

Radiometric performance of the APD and associated analog electronics was particularly important. Using Neyman–Pearson detection statistics, given the required detection probability ( $P_d = 0.95$ ) and false alarms ( $<10^{-2}$ ), our performance model indicates ranging operation well beyond the required 50 km (Fig. 12). At 232 km, our analysis indicates  $\approx 135$  equivalent signal photons ( $N_s$ ) arriving at the NLR detector (APD) surface, providing a detection probability  $P_d$  of 0.1 with false alarms of less than 0.01. Our detection scheme uses single-shot statistics; no multi-shot averaging is performed. At this range, we set the threshold level at  $7\sigma_0$  ( $\sigma_0$  is the receiver noise floor power level), providing a false alarm count of  $6 \times 10^{-4}$ . Figure 12 illustrates detection probability and the number of source photons received at the detector as a function of range to the asteroid.

Because the NLR uses leading-edge detection, pulse dilation due to interaction with the surface will introduce range error and can lead to performance loss as a result of receiver filter mismatch. This is especially true when we observe Eros at an angle,  $\theta_s$ , from nadir or when we range to a sloped surface ( $\theta_p$ , from the local horizon), or when significant surface roughness ( $Z_{rms}$ ) exists. Pulse dilation is defined as the temporal error in return pulse detection caused by elapsed time between the arrival of the initial and final backscattered photons for a given transmitter pulse, leading to error in measured TOF. Figure 13 illustrates these concepts for a divergence of  $\theta_d$ , nadir altitude  $h_0$ , mean slope of

$\theta_s$ , and an off-nadir look angle of  $\theta_p$ . An analysis<sup>10</sup> was performed that estimates pulse dilation as a range error,  $Z(\theta_s, \theta_p)$ , within a footprint. Figure 14 is a plot of  $Z(\theta_s, \theta_p)$  using values of pointing angles and a range of slope values presumed for the NLR mission. The loci where we match the science requirement of 6-m error are shown in Fig. 14.

Pulse dilation can also occur as the result of beam wave-front curvature or variations in localized surface albedo. Additional range errors can arise from electronic delay, timing errors, and incorrect correlation of attitude with range sample. Accounting for the various sources of range error with root-sum-square error analysis, we determined that the NLR instrument will generate a topographic field that is accurate to  $\approx 10$  m with respect to Eros's center of mass. (This is an estimate of the accuracy using the entire NLR data set within the ground-based data center. The NLR measures range to the asteroid's surface, not to its center of mass, which must be estimated through numerous measurements made while NEAR orbits Eros.)

## NLR TESTING

The NLR was tested at the instrument and spacecraft levels to ensure that it satisfied or exceeded all instrument and spacecraft requirements and that no adverse conditions existed that would jeopardize or corrupt spacecraft or other instrument operations. Instrument testing included functional, environmental, and end-to-end testing.

Functional testing used ground support equipment (GSE) to simulate return signals for the NLR to operate

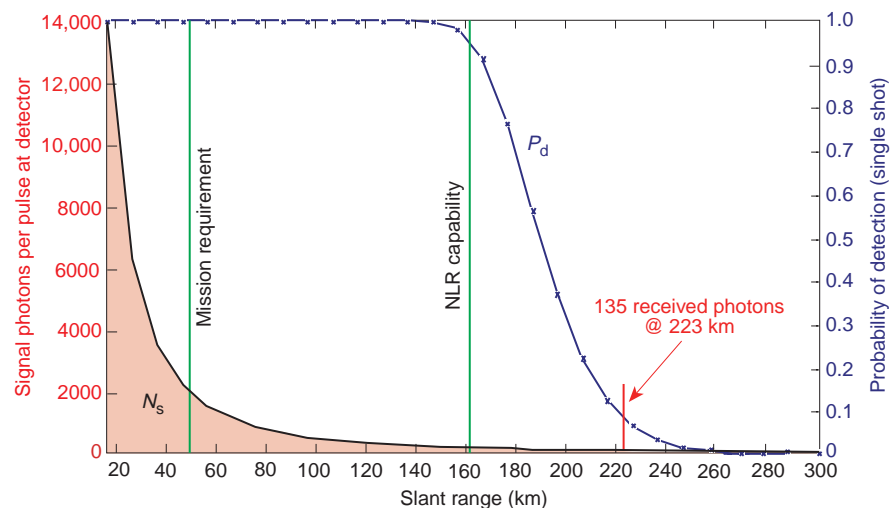


**Figure 12.** Plot of NLR performance based on parameter values describing Eros, mission geometry, and the NLR design. Avalanche photodiode output current was based on Webb's approximation. Probability of detection  $P_d$  indicates adequate operation beyond 50 km. At 223 km, analysis indicates  $\approx 135$  equivalent source photons ( $N_s$ ) arriving at the detector surface ( $P_d = 0.1$ ). Statistics assumed single-shot operation. False alarm was less than  $6 \times 10^{-4}$  using a threshold set at  $7 \times$  receiver noise floor ( $\sigma_0$ ).

with over simulated pulse-widths (dilation), return levels (simulating changes in range or albedo), and operational modes. Fiber-optic links allowed us to test throughout integration although the transmitter was a Class IV laser, which would have precluded open-air testing in unprotected areas.

Environmental testing was performed to evaluate the NLR operation and performance under various operating conditions (variable spacecraft bus voltages, environmental temperatures and gradients, and modes of operation). Because the NLR produces high currents within its power supply to the transmitter ( $\approx 45$  A), the influence on other spacecraft

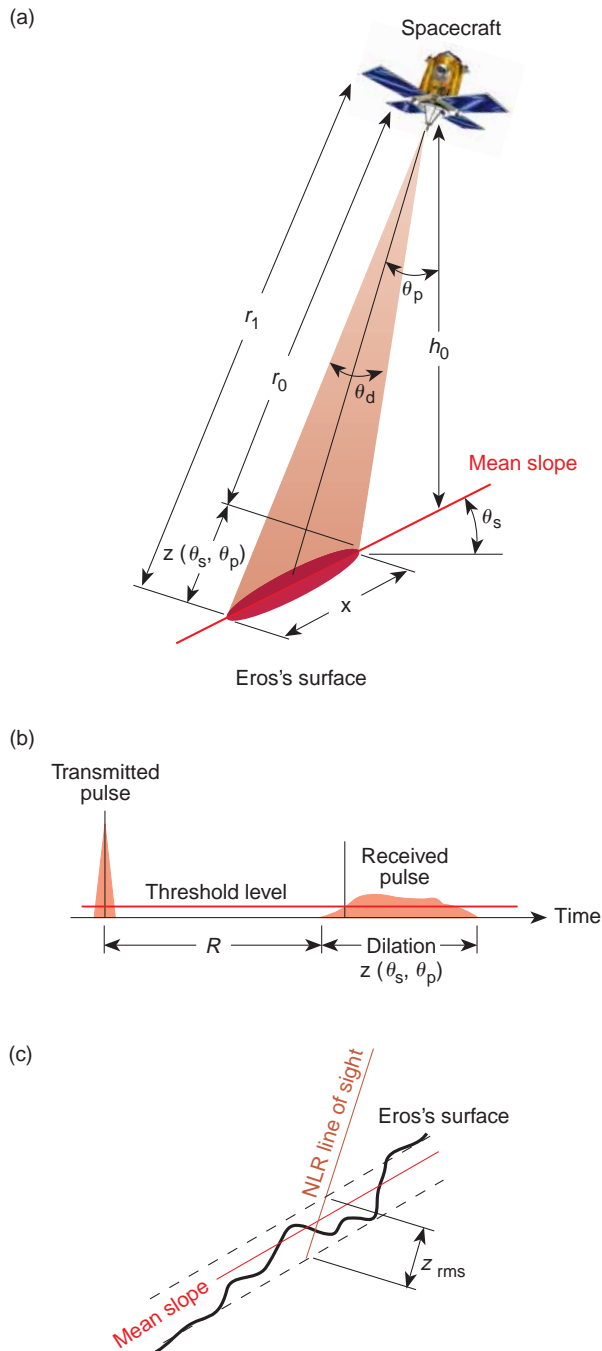


**Figure 13.** Diagram explaining pulse dilation occurring as the pulse interacts with the asteroid's surface. Various parameters describing the spacecraft's look angle are presented in (a), which give rise to pulse dilated returns, defined by (b). As the pulse is transmitted from the NLR, the pulse duration is relatively sharp and small,  $\approx 15$  ns. As the pulse incurs extended aspects of the surface, significant backscatter dilation starts to occur. This "distributed" return manifests itself by stretching the pulse over the finite extent of the range gate used. (c) The details associated with rough surface pulse stretching are shown.  $R$  = measured range;  $z_{rms}$  = surface roughness.

instruments (especially the magnetometer) was evaluated. No interference was observed from the NLR using data from all NEAR instruments during repeated

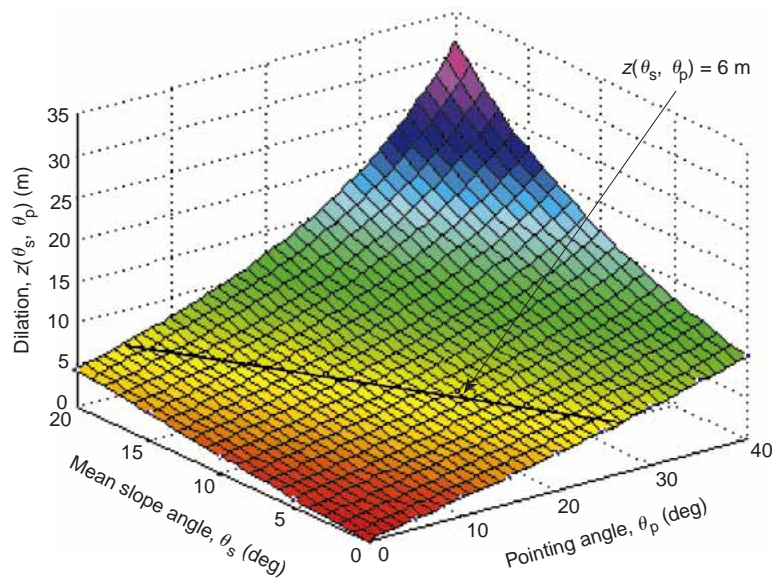
laser firings. This was verified during a post-launch interference test that was conducted in May 1996.

Finally, a free-space laser radar test was conducted to ensure end-to-end operation and to provide significant data and confidence in the ability of the NLR to perform as required. Prior to this test, the NLR had been operated using GSE; the receiver was provided with a "simulated" return signal, and the transmitter was used only to provide timing for the return signal. Issues such as power level sensitivity, optical alignment, and attributes associated with overall system implementation were not quantifiable until this end-to-end test was performed.

### Functional Testing

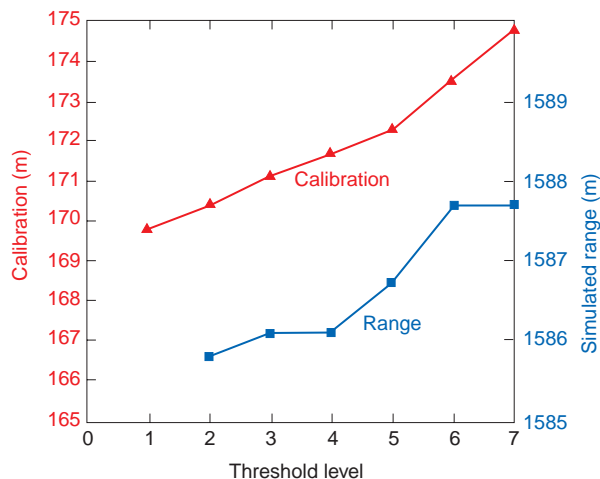
A graded-index lens was attached to one of the windows in the aperture door to provide access to the receiver prior to launch. A cap at the output aperture of the NLR transmitter was installed that had a fiber-optic connector to allow access to the laser. Fiber-optic links allowed direct access to the transmitter and receiver to permit simulation of effects during the environmental and functional tests without having to resort to open-air testing. This simulation allowed significant testing without affecting people around the laser, especially during spacecraft integration activities. Fiber optics routed the transmitted pulse from the laser to the GSE, where a photodetector converted the optical signal into an electrical one for simulation of delay, signal level changes, and pulse stretching. This modified signal was then sent to a GSE laser source, transforming the electrical signal back into an optical one. This modified optical signal could then be directed to the receiver, and NLR performance could be analyzed over a multitude of return signal conditions.

Figure 15 presents data for a functional test performed on the NLR. The receiver was sequenced through a range of threshold levels, and range counters were averaged over multiple laser firings at each of the threshold levels. The data plots in Fig. 15 illustrate an expected error caused by the use of leading-edge detection, a condition denoted as range-walk. As the threshold levels are increased, increasingly more energy is required by the return pulse to signal its arrival (which produces the STOP signal). Increased energy occurs later within the return pulse; thus the range indicated by the range counters increases with increased threshold levels, introducing a bias, or range-walk. The calibration curve shown in Fig. 15 illustrates a range-walk of 4 m over operational thresholds. The corresponding range-walk for range measurements is 2 m; the difference between the counters is that calibration measurements are one-way TOFs, whereas range is computed by dividing TOF by 2. In the particular case shown, calibration data at the lowest threshold were unreliable



**Figure 14.** Surface plot of dilation  $z(\theta_s, \theta_p)$  with locus of points describing  $z = 6$  m shown to indicate maximum permissible  $z$  (which becomes range error) for the NLR mission.

and therefore not plotted. For range, the measurements were excessively noisy at the lowest two levels, indicating insufficient energy in the return pulse for reliable detection. However, once we used threshold levels set for operation (levels from  $n = 2$  to  $n = 6$  in the threshold equation given earlier,  $2^n V_{th}$ ), reliable calibration and range values were provided by the tests.



**Figure 15.** Data for a functional test performed on the NLR. The receiver was sequenced through a range of threshold levels, and range counters were averaged over multiple laser firings at each of the threshold levels. The plots illustrate an expected error caused by the use of leading-edge detection, a condition denoted as range-walk. Threshold levels are described in the text and represent the binary exponent multiple of the base threshold voltage, 16 mV.

## Environmental Testing

To ensure that the instrument would survive launch stresses and the NEAR space environment, each NLR component was subjected to rigorous environmental testing. Such testing involved frequency-swept vibration levels, mechanically induced from 10 to 100 Hz at sweep rates of 4 octaves/min along the thrust-axis optical bore-sight. (Maximum amplitude of 15  $g$  occurred from 30 to 40 Hz.) Along the lateral axes, frequency range and rate were identical with maximum amplitudes occurring between 15 and 25 Hz of 7.5  $g$ . The NLR instrument was also subjected to random vibration over frequencies of 20–2000 Hz for 60 s with an overall root-mean-square amplitude of 13.6  $g$ .

Performance data were collected following each axis of vibration, and instrument alignment was verified before and after each test using two optical methods.

The first method measured the relative change between optical reference cubes mounted on the transmitter, receiver, and instrument base. The alignment of these reference cubes was measured with a theodolite having 2-arcsec precision. Transmitter-to-receiver alignment for our bistatic configuration was also determined by observing the transmitter beam in the receiver far-field FOV. This measurement was made by mapping the transmitter central lobe to the electronically determined FOV of the receiver. Measurements indicated that the shifts induced by the mechanical vibration tests (345  $\mu\text{rad}$ ) were well within the acceptable range (<1100  $\mu\text{rad}$ ), permitting reliable transmitter-to-receiver alignment.

The operating temperature of the spacecraft is projected to be between  $-29$  and  $+55^\circ\text{C}$ , and the survival range is projected to be between  $-34$  and  $+60^\circ\text{C}$ . However, manufacturers' specifications for some of the NLR elements required that the components be maintained at a different temperature range. This was accomplished through blanketing and heater control. We tested the adequacy of the NLR thermal design by testing the transmitter (laser) from 0 to  $+20^\circ\text{C}$ , the receiver optics from  $+10$  to  $+30^\circ\text{C}$ , and the NLR electronics from  $-29$  to  $+55^\circ\text{C}$ . Survival tests, during which the components are unpowered, increased the thermal range of operation testing by  $5^\circ\text{C}$  in each direction (e.g., transmitter survival testing range was increased to be from  $-5$  to  $+25^\circ\text{C}$ ).

To evaluate the NLR over these ranges, we placed the entire integrated instrument (including all power supplies and flight cabling) in a thermal-vacuum

(T-V) chamber and operated it over several thermal cycles. The T-V test lasted for 5 days: 3 days involved actual testing and 2 days were required to attain stable thermal and vacuum conditions for operation. To characterize the NLR while it was in the chamber, the previously described fiber-optic links were used to route the transmitter signal out of the chamber to the GSE and to return the modified optical signal back into the chamber to the receiver, permitting continuous performance evaluation. To prevent corona and to ensure reliable operation of the NLR, the instrument was soaked in vacuum ( $<10^{-5}$  torr) for the initial 36 h before it was powered.

We evaluated calibration data during the T-V testing, collecting over 200 range measurements at various threshold levels for each of the three plateau temperatures investigated,  $-29$ ,  $+25$ , and  $+55^{\circ}\text{C}$ . When operation at  $+55^{\circ}\text{C}$  was compared with operation at  $-29^{\circ}\text{C}$ , a very slight thermal influence on NLR performance was found; the range shifted by less than 0.5 ns ( $\approx 15$  cm).

### End-to-End System Test

An end-to-end system test, conducted under moderately controlled conditions in a 216.4-m-long hallway at APL, verified that the NLR operated as a laser altimeter system. The NLR was configured to fire at 1 Hz at two distinct targets, one at a time. One target, a sand-blasted aluminum sheet, could be characterized as a Lambertian scatterer. The second target, a silicate-rich rock, was used to represent more of what we expect of Eros's surface. Figure 16 shows these targets; the white circle on the targets in Fig. 16a is the actual Nd:YAG infrared beam; the camera used to photograph is a charge coupled device camcorder and is sensitive to the near infrared. Data were collected at one range for the aluminum target and at two separate ranges for the rock target. Target ranges varied between 182 and 211 ft, with actual values determined using a NIST-traceable 91.44-m surveyor's rule. The data, as represented in Fig. 16a, illustrate the insignificant noise and error levels associated with NLR operation.

To simulate actual operating distances (nominally 50 km) for the NLR, we used neutral density filters

and an aperture stop for a total attenuation of 71 dB. The graphs in Fig. 16 show range data from the NLR for operational threshold levels. As expected, at the lowest threshold levels noise dominated, and at the highest threshold levels no returns were detected.

Given the binary-increasing (octave) scaling used to create the threshold levels (recall that comparator voltage levels vary as  $2^n V_{\text{th}}$ ), the operational threshold at  $n = 5$  is  $\approx 9$  dB above the receiver noise floor. With the 71-dB attenuation, estimated link margin for the NLR operating at 50 km to Eros is estimated to be 9–12 dB. The 3-dB granularity cannot be improved upon using these test data because the data were taken using the eight-valued preset threshold scheme.

### SUMMARY

The successful launch of the NEAR spacecraft from Cape Canaveral on 17 February 1996 at 3:43 EST was only the beginning. Three tests performed subsequent

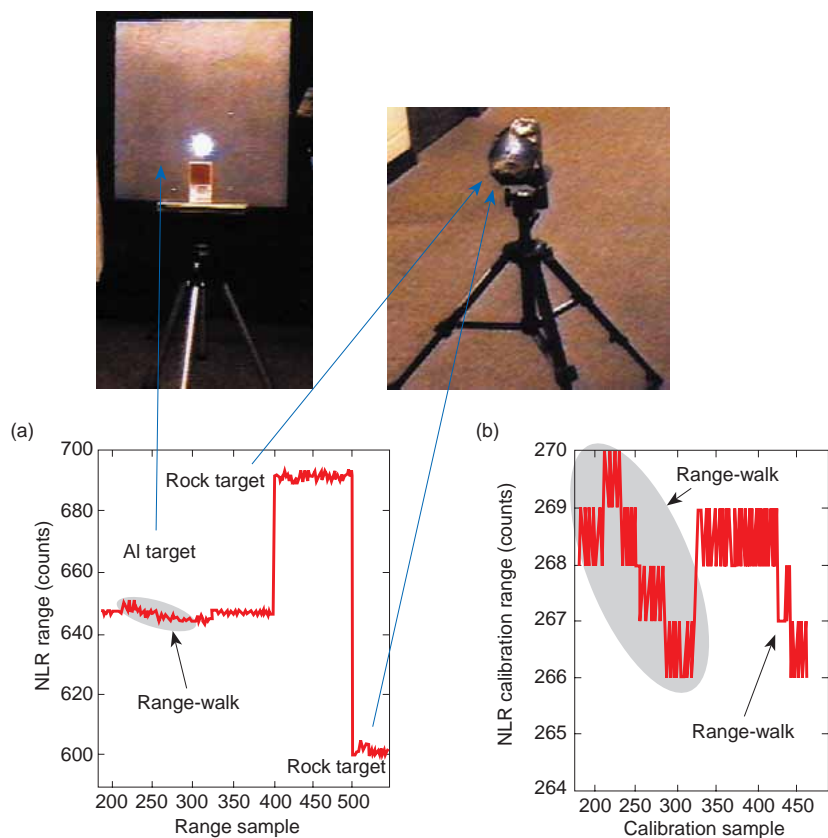


**Figure 16.** A free-air test (in a 216.4-m hallway) within the APL campus. (a) Evaluation and (b) calibration of NLR. Photographs of the targets used (sand-blasted aluminum and silicate rock) are also shown. The arrows indicate which target was illuminated during data collection. (a) Note the presence of the infrared laser beam on the targets as a result of the infrared sensitivity of the “photographs,” which were derived from frames of a commercial charge coupled device camcorder. (b) An expanded version of the threshold changes while the aluminum target was viewed (the plots in a and b are time correlated). Counts are converted to range by using the speed of light,  $c$ . (Calibration requires division by an index of refraction of the fiber optic,  $\approx 1.5$ ; range uses  $c$ , but must be divided by 2 to account for round-trip elapsed time.)

to launch indicated satisfactory operation of the NLR. The actual Eros rendezvous is scheduled for February 1999. From the substantial surface coverage of Eros by the NLR and the altimeter's expected resolution and accuracy performance, the resulting measurements should significantly enhance our understanding of asteroid structure. In addition to instrument-level testing, the NLR underwent spacecraft qualification testing as an integrated instrument. Figure 17 depicts the NLR located on the NLR instrument deck (note the nonflight, red caps that were used to protect the optics prior to launch).

Although the NLR was a relatively simple laser radar compared with designs commonly in use by terrestrial laser rangefinders, the combined requirement of operating an instrument in deep space for a prolonged period under strong design constraints (weight, cost, and schedule) contributed significantly to the complexity of this instrument. Fortunately, radiation effects for the NEAR mission are slight (10-krad total dose); nevertheless, space exposure influenced our selection and design approach for the electronics and the optical components.

#### REFERENCES

- <sup>1</sup> Binzel, R., Gehrels, T., and Matthews, M. (eds.), *Asteroids II*, The University of Arizona Press, Tucson (1989).
- <sup>2</sup> *Near Earth Asteroid Rendezvous Laser Transmitter, Vol. 1: Technical and Management*, Proposal to RFP No. 389, McDonnell Douglas Aerospace—West (13 Dec 1993).
- <sup>3</sup> Bass, M. (ed.), *Handbook of Optics, Vol. 1: Fundamentals, Techniques, and Design*, McGraw-Hill, New York (1995).
- <sup>4</sup> Swenson, T., *Specification of Microplasma 1064-nm Narrow Band Filter*, Technical Application Note, Optical Corp. of America (29 Aug 1994).
- <sup>5</sup> Davidson, F. M., and Sun, X., *Reduced Electrical Bandwidth Receivers for Direct Detection 4-ary PPM Optical Communication Intersatellite Links*, NASA Final Report, Grant NAG5-1510 (Feb 1993).
- <sup>6</sup> Reiter, R. A., *Timing Precision of the NEAR Navigation Laser Rangefinder (NLR) Analog Electronics*, APL Technical Memorandum S2A-93-0201, JHU/APL, Laurel, MD (27 Sep 1993).
- <sup>7</sup> Rodriguez, D., *NEAR Laser Rangefinder Digital Processor—Electrical Design Data Package*, APL Technical Memorandum S2F-94-0315, JHU/APL, Laurel, MD (6 Oct 1994).
- <sup>8</sup> Moore, R. C., *NEAR NLR Flight Software Requirements Specification*, APL Technical Report 7352-9069, JHU/APL, Laurel, MD (Oct 1994).
- <sup>9</sup> Webb, P. P., "Properties of Avalanche Photodiodes," *RCA Rev.* 234-278 (Jun 1974).

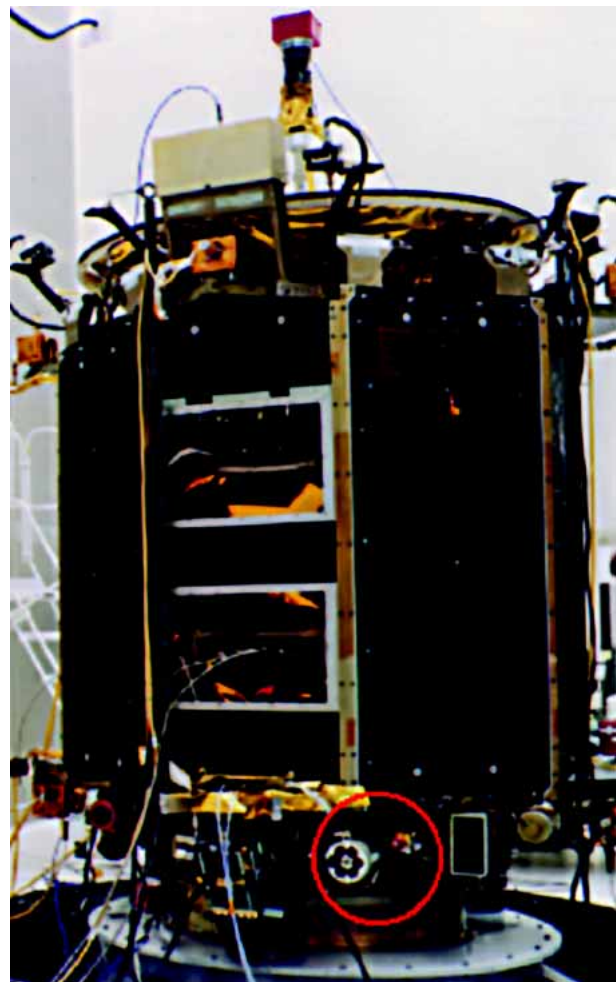


**Figure 17.** The NLR instrument (circled) as integrated into the NEAR spacecraft. Note the red-tag covers used to protect optics prior to launch. The total spacecraft mass was 816.5 kg (1800 pounds) (with propellant); the NLR weighed slightly less than 5 kg.

- <sup>10</sup> Cole, T. D., and Davidson, F. M., "Performance Evaluation of the Near-Earth Asteroid Rendezvous (NEAR) Laser Rangefinder," *Proc. SPIE, Photonics for Space Environments IV* 2811, 156-168 (1996).

ACKNOWLEDGMENT: This work was supported under contract N00039-95-C-002 with the U.S. Navy. Thomas B. Coughlin is the program manager for the NEAR program.

#### THE AUTHOR



TIMOTHY D. COLE is the section supervisor of the Electro-Optical Instrumentation Section within APL's Space Department. He holds academic degrees in electrical engineering (B.S.E., M.S.E.E.) and technical management (M.S.). Mr. Cole has been involved in laser radar technologies for both exoatmospheric and terrestrial applications. He designed and led the engineering effort that developed the NEAR laser altimeter. He has also been a lead engineer and project manager on several space programs and led the development of an ophthalmologic instrument in collaboration with the Hopkins Wilmer Eye Institute. Before Mr. Cole came to APL, he performed analyses of and research into long-wave infrared sensors and detector technologies. Currently, he is a member of the NLR science team and holds a chair position at the Center for Non-destructive Evaluation (CNDE). His e-mail address is timothy.cole@jhuapl.edu.